

Molecular Hydrogen in the Extremely Metal-Poor, Star-Forming Galaxy Leo P

O. Grace Telford^{1,2,3}, Karin M. Sandstrom⁴, Kristen B. W. McQuinn^{3,5},
Simon C. O. Glover⁶, Elizabeth J. Tarantino⁵, Alberto D. Bolatto^{7,8},
Ryan J. Rickards Vaught^{4,5}

¹Department of Astrophysical Sciences, Princeton University, 4 Ivy Lane, Princeton, NJ 08544, USA; grace.telford@princeton.edu.

²The Observatories of the Carnegie Institution for Science, 813 Santa Barbara Street, Pasadena, CA 91101, USA.

³Department of Physics and Astronomy, Rutgers University, 136 Frelinghuysen Road, Piscataway, NJ 08854, USA.

⁴Department of Astronomy & Astrophysics, University of California, San Diego, La Jolla, CA 92093, USA.

⁵Space Telescope Science Institute, 3700 San Martin Drive, Baltimore, MD 21218, USA.

⁶Universität Heidelberg, Zentrum für Astronomie, Institut für Theoretische Astrophysik, Albert-Ueberle-Str. 2, D-69120 Heidelberg, Germany.

⁷Department of Astronomy, University of Maryland, College Park, MD 20742, USA.

⁸Joint Space-Science Institute, University of Maryland, College Park, MD 20742, USA.

The James Webb Space Telescope (JWST) has revealed unexpectedly rapid galaxy assembly in the early universe, in tension with models of star and galaxy formation [1–3]. In the gas conditions typical of early galaxies, particularly their low abundances of heavy elements (metals) and dust, the star-formation process is poorly understood. Some models predict that stars form in atomic gas at low metallicity [4, 5], in contrast to forming in molecular gas as observed in higher-metallicity galaxies [6]. To understand the very high star-formation rates at early epochs, it is necessary to determine whether molecular gas formation represents a bottleneck to star formation, or if it is plentiful even at extremely low metallicity. Despite repeated searches [7], star-forming molecular gas has not yet been observed in any galaxy below 7% of the Solar metallicity [8], leaving the question of how stars form at lower metallicities unresolved. Here, we report the detection of rotationally excited emission from molecular hydrogen in the star-forming region of the nearby, 3% Solar metallicity galaxy Leo P [9, 10] with the MIRI-MRS instrument onboard JWST. These observations place a lower limit on the molecular gas content of Leo P and, combined with our upper limit on carbon monoxide emission from a deep search of this galaxy, demonstrate that MIRI-MRS is sensitive to much smaller molecular gas masses at extremely low metallicity compared to the traditional observational tracer. This discovery pushes the maximum metallicity at which purely atomic gas may fuel star formation a factor of two lower, providing crucial empirical guidance for models of star formation in the early universe.

Observations in the local universe show that star formation occurs in molecular gas in metal-rich galaxies [11, 12]. While molecular hydrogen (H_2) is the most abundant molecule in these clouds, its lack of an electric dipole moment and low moment of inertia mean that it does not produce observable emission at low temperatures ($\lesssim 100$ K). Emission from carbon monoxide (CO) is therefore widely used to trace star-forming, cold molecular gas clouds, but the correlation between H_2 mass and CO luminosity

breaks down at low metallicities. The changing balance between CO formation and destruction, primarily driven by the lower dust content of metal-poor gas, combined with the self-shielding of H₂ results in a smaller CO-emitting region for a molecular cloud of fixed H₂ mass and consequently a lower observed CO intensity [13–15]. The non-detection of CO in star-forming galaxies below 7% of the Solar value [e.g., 7] therefore does not elucidate whether stars can form directly from cold atomic hydrogen (H I) instead of H₂ in metal-poor environments, as predicted by some models [4, 5].

The temperature of H₂ in star-forming regions ranges from < 10 K in the cold, dense cores of molecular clouds up to several hundred K in their outer layers, where the gas is heated by ultraviolet radiation from short-lived massive stars. Because rotational H₂ lines can be collisionally excited in these photodissociation regions (PDRs), it is possible to observe emission from the warm phase of H₂, which constitutes ~10–15% of the total H₂ mass in typical star-forming galaxies across a wide range of metallicities [16, 17]. Such mid-infrared H₂ emission lines have been detected in moderately metal-poor dwarf galaxies with the Spitzer Space Telescope [e.g., 18, 19], but observations of warm H₂ remain elusive for star-forming galaxies at extremely low metallicity [i.e., below 5% Solar; 20]. It is unclear whether this is because the rotationally excited emission lines are below the sensitivity limit of existing observations or due to a true lack of H₂. CO-emitting molecular clouds are very compact ($\lesssim 2$ pc) at low metallicity [8, 21], suggesting that any emission from molecular gas could be strongly diluted in low-angular-resolution data. JWST’s powerful combination of wavelength coverage in the mid-infrared, high spatial resolution, and more sensitive detectors compared to earlier mid-infrared telescopes has opened the possibility of detecting H₂ emission from an extremely low-metallicity galaxy that is close enough to be spatially resolved.

The 3% Solar metallicity dwarf galaxy Leo P is among the most metal-poor star-forming galaxies known in the local universe [9]. Despite its low star-formation rate ($4.3 \times 10^{-5} M_{\odot} \text{ yr}^{-1}$; Table 1), the presence of just one O-type star (lifetime $\lesssim 10$ Myr) and several other blue, massive stars unambiguously confirms that Leo P is actively forming stars [22]. The O star, which powers the only H II region in the galaxy, has been studied in detail with multiwavelength observations that show it has a modest effective temperature of 34 kK, a high rotation rate, and a weak stellar wind [23–25]. Leo P is isolated and has been forming stars at a relatively constant rate over its lifetime [10, 26], in contrast to similarly metal-poor galaxies like I Zw 18 [27] and SBS 0335–052 [28], which are experiencing bursts of star formation (possibly induced by recent mergers) and therefore have complex and intense radiation fields. Moreover, these metal-poor starbursts are quite distant; Leo P is over 10 times closer, just 1.6 Mpc away. Its proximity and simple star-forming environment present a unique opportunity to observe the star-formation process at the very low metallicities typical of galaxies in the early universe at high spatial resolution.

Leo P’s gaseous components have been thoroughly studied via H I 21-cm emission [29, 30] and CO observations [7], which failed to detect molecular gas down to a CO luminosity limit of $L_{\text{CO}} \leq 2900 \text{ K km s}^{-1} \text{ pc}^2$. This motivated us to conduct deeper observations of Leo P with the Atacama Large Millimeter Array (ALMA), which again resulted in a non-detection, but placed an upper limit on the molecular gas content two orders of magnitude more stringent: $L_{\text{CO}} \leq 43.6 \text{ K km s}^{-1} \text{ pc}^2$ (see Table 1 and Methods). Yet, because the ratio of molecular gas mass to CO luminosity (α_{CO}) is expected to be large at low metallicity [e.g., 4, 31], this deep limit on L_{CO} still allows for up to $1.2 \times 10^4 M_{\odot}$ of H₂. Not even these state-of-the-art ALMA data can confirm or conclusively rule out molecular gas in Leo P.

We then observed Leo P with JWST’s MIRI-MRS instrument to search for emission from rotationally excited H₂ (see Methods). Figure 1 shows a Hubble Space Telescope image of Leo P in greyscale, with blue contours showing the distribution of H I from Very Large Array 21-cm observations [30]. The region that we searched with ALMA for CO emission is shown as the red circle. The inset image shows a map of the [Ne III] $\lambda 15.6 \mu\text{m}$ nebular line intensity constructed from the MIRI-MRS channel 3 data cube, where a spectrum spanning 11.55–17.98 μm is measured in each spaxel (or spatial pixel). This line is among the brightest in the MIRI-MRS data, and H II region is visible as the highest-intensity (pink/yellow) spaxels.

We searched the channel 3 data for the H₂ S(1) emission line at 17.03 μm , which is expected to be the most easily detectable of the mid-infrared H₂ rotational transitions (see Methods). This revealed H₂ S(1) emission detected above the 3- σ level across six contiguous spaxels near the H II region, unambiguously confirming the presence of molecular gas in the star-forming region of this extremely metal-poor galaxy. The total area of those six spaxels (each 0.2'' on a side) is slightly smaller than the area of one spatial resolution element at 17 μm (0.67'' full width at half maximum, or FWHM). Thus, we use the center of those six spaxels to define the location of the unresolved H₂ S(1) emission, and adopt a diameter equal to the FWHM at 17 μm ; see the white open circle in the inset image of Figure 1. At the distance of Leo P,

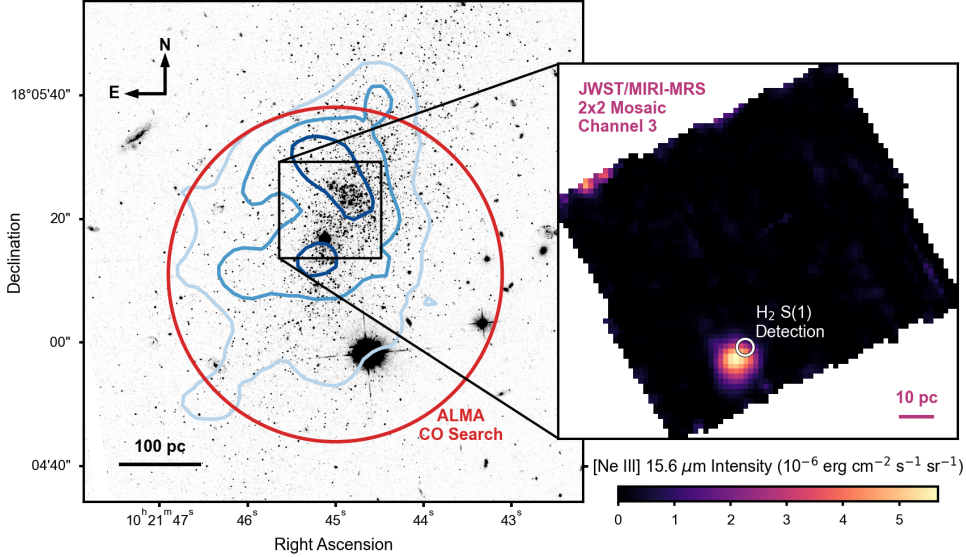


Fig. 1 Warm H_2 emission detected in Leo P’s star-forming region. A Hubble Space Telescope image of Leo P in the F475W filter [10] is shown in greyscale with contours overlaid to show H I column densities at $8''$ resolution, where values of 1.6 , 2.8 , and $4.0 \times 10^{20} \text{ cm}^{-2}$ correspond to increasingly darker shades of blue [30]. The bright H II region is visible as the black circular region just north of the southern peak in the H I column density. The red circle indicates the field of view of our ALMA observation that placed a deep upper limit on the CO luminosity (see Table 1 and Methods). The inset image shows a map of the $[\text{Ne III}] \lambda 15.6 \mu\text{m}$ nebular emission line constructed from our JWST MIRI-MRS channel 3 data cube, where the ionized gas in the H II region produces the brightest emission (pink/yellow colors). The white open circle encloses the region where the rotationally excited H_2 S(1) line at $17.03 \mu\text{m}$ is detected in the MIRI-MRS observations (Figure 2).

this corresponds to a warm H_2 cloud with a maximum equivalent radius of 2.6 pc , similar to the small sizes of the lowest-metallicity cold molecular gas cores detected in CO observations to date [8, 21]. The H_2 S(1) emission is detected at the northwestern edge of Leo P’s only H II region, consistent with being produced in a classic PDR: a transition zone where the ionized gas meets an H_2 -bearing cloud.

The left panel of Figure 2 presents a portion of the channel 3 MRS spectrum around the H_2 S(1) line, averaged over the region in which that line is detected (white circle in Figure 1). We measure the line intensity as the area under a Gaussian model (purple) fit to the observed line profile (black), which is securely detected with a signal-to-noise ratio (SNR) of 5.3 (see Methods). In addition to the S(1) line, our MIRI-MRS observations cover the wavelengths of three other H_2 rotational lines arising from excited states of different energies. The center panels of Figure 2 show the channel 2 (top) and channel 3 (bottom) MRS spectra in the same spatial region as the S(1) detection centered on the S(3) and S(2) transitions at $9.66 \mu\text{m}$ and $12.28 \mu\text{m}$, respectively. Neither line is formally detected at $\text{SNR} > 3$, but we use the intensity measurement uncertainties to place $3\text{-}\sigma$ upper limits on both lines (see Table 1). Unfortunately, the noise level is so high at the reddest wavelengths ($\gtrsim 24 \mu\text{m}$ in channel 4) that we cannot obtain a useful limit on the S(0) $28.22 \mu\text{m}$ line, which probes the coldest H_2 that can emit in the mid-infrared.

The measured S(1) intensity of $6.3 \times 10^{-7} \text{ erg s}^{-1} \text{ cm}^{-2} \text{ sr}^{-1}$ is strikingly low. To produce such weak emission, either the column density of the emitting warm H_2 gas must be orders of magnitude lower than typically observed in molecular clouds ($\gtrsim 10^{20} \text{ cm}^{-2}$) [6], or the temperature of the warm H_2 component must be very low. The right panel of Figure 2 shows how the measured S(1) intensity and S(2) and S(3) upper limits constrain the temperature and total column density of the emitting warm H_2 (see Methods). Black points with error bars (or arrows, for limits) show the column density in the upper energy level of each transition (N_u), calculated from the line intensity measurements and normalized by the statistical weight (g_u), as a function of the upper level energy (E_u) divided by the Boltzmann constant (k_B). The two colored lines show single-temperature models that bound the range of parameters allowed by the data: the blue model has a cold temperature of 80 K and an associated total column density of $5.2 \times 10^{21} \text{ cm}^{-2}$, while the red model has a higher temperature of 420 K , and consequently, a total column density nearly four orders of magnitude smaller. If radiative heating by Leo P’s only O star dominates the heating of the observed H_2 , then modeling of the PDR suggests a temperature close to the lower end of this range

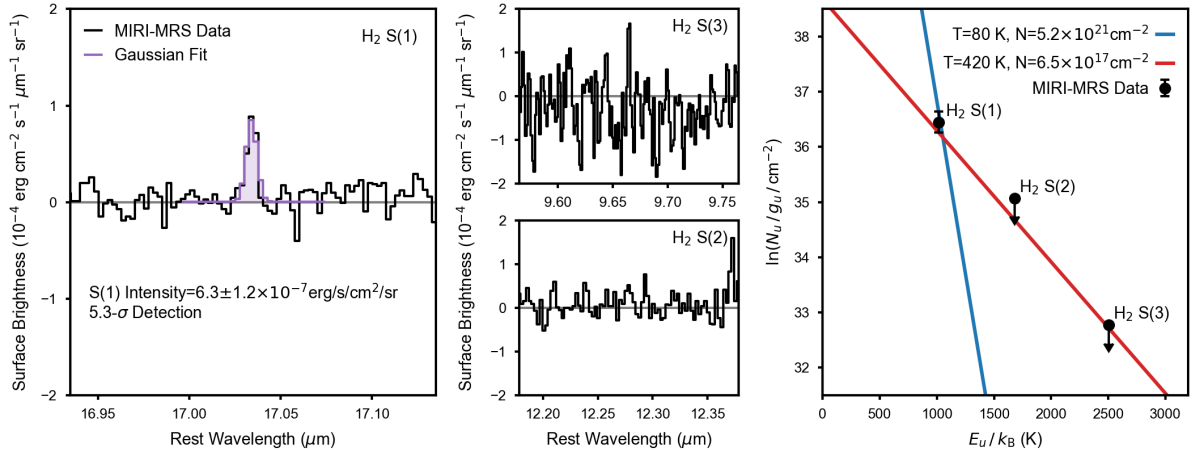


Fig. 2 Constraints on the warm H₂ properties in Leo P. *Left:* Shown in black is the average observed MIRI-MRS spectrum within the region indicated by the white circle (0.67'' diameter) in the inset image in Figure 1, centered on the wavelength of the H₂ S(1) transition. The best-fit Gaussian model to the data within ± 700 km s⁻¹ of the line center, from which the line intensity is measured, is shown in purple. *Center:* The average MIRI-MRS spectrum in the same region, now centered on the S(3) and S(2) lines in the top and bottom panels, respectively. Neither line is significantly detected in the observations. *Right:* black points show the column density in the upper level of each H₂ transition (N_u), calculated from the measured line intensity or 3- σ upper limits (arrows) and normalized by the statistical weight (g_u), as a function of the upper level energy expressed as an equivalent temperature (E_u/k_B). The blue and red lines show the range of single-temperature models consistent with the data (see Methods), with associated temperature (T) and total column density (N) of warm H₂ reported in the legend. The model in blue adopts the lowest temperature at which detectable H₂ S(1) emission is expected, while the model in red is that with the highest temperature consistent with both the S(1) intensity and S(3) upper limit.

(see Methods for model details). However, cosmic ray heating or the dissipation of turbulent motions in shocks could potentially yield a higher temperature.

Importantly, because a higher-temperature warm H₂ cloud with a lower total column density would be inconsistent with the MIRI-MRS data, warm H₂ with a column density of at least 6.5×10^{17} cm⁻² (corresponding to a temperature of 420 K) must be present in Leo P. This implies a minimum warm H₂ mass of $0.2 M_\odot$ within the single spatial resolution element where the S(1) emission line is detected (white circle in Figure 1), which has a physical area of 21.7 pc². While this is quite a small gas mass, it is merely a lower limit; if the emitting warm H₂ is indeed at a colder temperature of 80 K, then the required higher column density would translate to a warm H₂ mass of $1.8 \times 10^3 M_\odot$. Moreover, the observational result that just ~ 10 – 15% of the total H₂ mass is in the warm phase in typical star-forming galaxies [16, 17] suggests that the minimum total (warm+cold) H₂ mass in Leo P is at least 6.5–10 times larger than the lower limit on the warm H₂ mass, or $\geq 1.4 M_\odot$. If the warm H₂ is indeed at 80 K (i.e., at the lowest end of the temperature range expected to produce S(1) emission), then its higher column density would imply a total H₂ mass of at least $1.1 \times 10^4 M_\odot$, which is at the high end of the range of virial masses ($\sim 10^3$ – $10^4 M_\odot$) reported for CO-detected molecular clouds in the metal-poor galaxies WLM and Sextans B [8, 21]. Even this higher H₂ mass implied by the observed rotational line emission is fully consistent with the upper limit on the H₂ mass of $1.2 \times 10^4 M_\odot$ from our deep ALMA observations (see Methods), but if the emitting gas is at a higher temperature, the H₂ mass in Leo P may be orders of magnitude smaller. The relatively large upper limit is due to the combination of the larger ALMA beam size, which may dilute emission from compact CO-emitting clouds [8, 21], with the high values of α_{CO} expected at low metallicity [4, 31]. The much lower H₂ mass to which our JWST observations are sensitive emphasizes the power of MIRI-MRS as a new tool to detect H₂ in extremely metal-poor galaxies.

Confirmation of H₂ in the star-forming region of Leo P disfavors models in which stars can form in purely atomic gas at 3% Solar metallicity. This result provides a valuable constraint on the physics of star formation in the early universe, where the population of surprisingly bright galaxies recently revealed by JWST have posed a major challenge to existing models of galaxy assembly [e.g., 1–3]. Our observations in Leo P show empirically that H₂ does form even at the extremely low metallicities ($\leq 5\%$ Solar) observed in many early galaxies [e.g., 32, 33], an important benchmark for accurately modeling the cooling and chemistry of star-forming gas in that regime. These findings also support the use of models that tie star formation to H₂ in galaxy formation simulations [e.g., 34, 35] during the early stages of assembly, and for low-metallicity dwarf galaxies at all cosmic epochs.

Table 1 Observed and Derived Quantities for Leo P

Galaxy Properties	
H II Region Right Ascension (J2000)	10:21:45.1217
H II Region Declination (J2000)	+18:05:16.93
Distance D (Mpc)	1.62 ± 0.15
Physical size of 1 arcsec at D (pc)	7.85 ± 0.73
Systemic Velocity v_{sys} (km s^{-1})	260.8 ± 2.5
Metallicity $12 + \log(\text{O}/\text{H})$	7.17 ± 0.04
Stellar Mass M_{\star} (M_{\odot})	$2.7 \pm 0.4 \times 10^5$
H I Mass M_{HI} (M_{\odot})	8.1×10^5
Star Formation Rate $\text{SFR}_{\text{H}\alpha}$ ($M_{\odot} \text{ yr}^{-1}$)	4.3×10^{-5}
ALMA Observations (Project 2013.1.00397.S)	
Field of View Right Ascension (J2000)	10:21:45.0000
Field of View Declination (J2000)	+18:05:11.00
Primary Beam FWHM (arcsec)	54.13
Restoring Beam FWHM (arcsec)	3.02×2.10
Velocity Resolution (km s^{-1})	0.25
L_{CO} ($\text{K km s}^{-1} \text{ pc}^2$)	≤ 43.6
$M_{\text{H}_2}^{\text{cold}}$ assuming $\alpha_{\text{CO}} = 285$ (M_{\odot})	$\leq 1.2 \times 10^4$
MIRI-MRS Observations (JWST-GO-3449)	
H ₂ S(1) Detection Right Ascension (J2000)	10:21:45.1076
H ₂ S(1) Detection Declination (J2000)	+18:05:17.46
Resolution Element FWHM at $17 \mu\text{m}$ (arcsec)	0.67
H ₂ S(1) Intensity ($\text{erg s}^{-1} \text{ cm}^{-2} \text{ sr}^{-1}$)	$6.3 \pm 1.2 \times 10^{-7}$
H ₂ S(2) Intensity ($\text{erg s}^{-1} \text{ cm}^{-2} \text{ sr}^{-1}$)	$\leq 5.4 \times 10^{-7}$
H ₂ S(3) Intensity ($\text{erg s}^{-1} \text{ cm}^{-2} \text{ sr}^{-1}$)	$\leq 9.1 \times 10^{-7}$
Warm H ₂ Temperature T (K)	≤ 420
Warm H ₂ Column Density N (cm^{-2})	$\geq 6.5 \times 10^{17}$
Warm H ₂ Mass $M_{\text{H}_2}^{\text{warm}}$ (M_{\odot})	≥ 0.2
Warm H ₂ Mass if $T = 80 \text{ K}$ (M_{\odot})	1.8×10^3

References for galaxy properties: [9, 10, 23, 26, 29, 30, 36]. Right ascension is reported in hours, minutes, seconds, and declination in degrees, arcminutes, arcseconds. $\alpha_{\text{CO}} = 285$ is a conservatively large predicted value at 3% Solar metallicity [4] (see Methods).

Methods

JWST MIRI-MRS Observations and Data Reduction

We designed JWST program GO-3449 (PI: O. G. Telford) to detect, or place stringent upper limits on, rotationally excited transitions of warm H₂ in Leo P. These mid-infrared lines at $9.6\text{--}28.2 \mu\text{m}$ (see Table 2) fall within the wavelength coverage of the the Mid-Infrared Instrument (MIRI)[37, 38]. We used MIRI’s Medium Resolution Spectroscopy (MRS) observing mode [39, 40] to achieve the spectral resolution necessary for faint emission-line measurements. MIRI-MRS observations are split across 4 integral field units, or channels, where the covered wavelengths increase, the field of view gets larger, and the spatial resolution and sampling get coarser from channels 1 to 4 (see the MIRI-MRS documentation¹ for details). In each channel, the wavelength coverage is divided into 3 bands (A/SHORT, B/MEDIUM, and C/LONG), and a given band within all 4 channels is observed simultaneously. The H₂ lines of interest span bands A, B, and C, so we observed Leo P in all 3 bands to cover the full wavelength range accessible to MIRI-MRS.

Our aim was to search for H₂ emission across all regions in Leo P where the emission was likely to be seen, particularly where young stars and the H II region are found and near the highest observed column densities of H I (see Figure 1). Because the S(1) line at $17.03 \mu\text{m}$ is expected to be detectable across the widest range of possible warm H₂ temperatures, we selected channel 3 as the primary for mosaic construction (with 10% overlap between adjacent pointings). Good coverage of Leo P required 4 pointings to construct a 2×2 mosaic, given the size of the channel 3 field of view. We used the SLOWR1 readout

¹<https://jwst-docs.stsci.edu/jwst-mid-infrared-instrument/miri-observing-modes/miri-medium-resolution-spectroscopy>

Table 2 H₂ Rotational Lines

H ₂ Line Name	Transition ($\nu = 0$)	Wavelength (μm)	MIRI-MRS Channel	MIRI-MRS Band	E_u/k_B (K)	g_u	A (10^{-11} s^{-1})
S(0)	$J(2-0)$	28.22	4	C	510	5	2.94
S(1)	$J(3-1)$	17.03	3	C	1015	21	47.6
S(2)	$J(4-2)$	12.28	3	A	1682	9	276
S(3)	$J(5-3)$	9.66	2	B	2504	33	984

From left to right, the columns report the following parameters used in our observational design and modeling: the short name of each transition; the upper and lower rotational quantum numbers (J); the rest wavelength; the MIRI-MRS channel in which the line falls; the MIRI-MRS band; the energy of the upper level expressed as an equivalent temperature; the statistical weight of the upper level; and the Einstein coefficient. Values compiled from [43].

pattern, adopted the 4-pt dither pattern optimized for extended sources to improve PSF sampling, and obtained a background observation for each band.

To determine the exposure time necessary to place a 5- σ limit on the H₂ S(1) line, we calculated the expected intensity for a total (warm+cold) H₂ column density of 10^{21} cm^{-2} with a 10% warm fraction and temperature of 120 K, typical of the temperatures and fractions found by the SINGS survey [16]. These assumptions gave a predicted intensity of $6.6 \times 10^{-7} \text{ erg s}^{-1} \text{ cm}^{-2} \text{ sr}^{-1}$. Using this limiting S(1) intensity in the JWST exposure time calculator² (ETC, v.2), and adopting 12 groups per integration to stay below the 300s limit recommended to mitigate the impacts of cosmic rays, we found that 2 integrations (times the 4 exposures in the dither pattern, for 8 total integrations) were required to reach S/N = 5. In total, this resulted in a total exposure time of 2389s for MIRI-MRS band C at each pointing; 4 in the mosaic to cover Leo P, plus 1 background observation. Because the predicted intensities of the other lines are more sensitive to the warm H₂ temperature, we adopted the same exposure time across all 3 bands for consistency and expected to place weaker limits on the S(0), S(2), and S(3) emission.

The MIRI-MRS observations of Leo P executed on May 23, 2024. We retrieved the `uncal` images from the Mikulski Archive for Space Telescopes (MAST) and processed them using version 1.15.1 of the JWST calibration pipeline with the CRDS context `rwst1281.pmap` [41]. Our reduction followed the steps in the MIRI-MRS batch processing notebook by D. Law, retrieved from GitHub in July 2024³. We used a pixel-based background subtraction and processed the Leo P observations through the `Detector1`, `Spec2`, and `Spec3` stages of the pipeline. We built the cubes in “ifualign” coordinates, to later allow for additional row-based background corrections. Similar to the results presented in [42], we found residual stripe artifacts in our reduced MIRI-MRS observations in all four channels. These may be related to imperfect cosmic ray shower removal or to striping and/or detector noise [40]. To remove these, again similar to [42], we selected ~ 5 signal-free columns of the cube and found a row-based average background level in each wavelength slice of the cube. This additional background removal resulted in improved noise characteristics. We note that the details of this background subtraction are not critical to the detection of narrow emission lines—we detect H₂ S(1) at similar S/N with or without the additional row-based background subtraction. It does, however, improve the noise characteristics of the cube and enable more stringent limits on the non-detected H₂ lines.

Emission-Line Flux Measurements

Of the four pure rotational H₂ transitions (with no change in the vibrational quantum number $\nu = 0$; see Table 2) covered by our MIRI-MRS observations, the S(1) transition is expected to be detectable across the widest range of possible temperatures. Thus, we began by searching individual spaxels in the channel 3 data cube for S(1) emission at $17.03 \mu\text{m}$. We modeled the wavelengths within $\pm 700 \text{ km s}^{-1}$ (corresponding to $\pm 0.04 \mu\text{m}$) of the expected observed wavelength of this transition, accounting for Leo P’s systemic velocity of 260.8 km s^{-1} , as a constant continuum level plus a Gaussian emission line. MIRI-MRS’s spectral resolution ($R \sim 2400\text{--}3400$ over the wavelengths of the H₂ rotational lines, corresponding to a velocity FWHM of $\sim 90\text{--}120 \text{ km s}^{-1}$) is insufficient to resolve the expected narrow line width of molecular gas. Indeed, even emission lines produced in Leo P’s H II region, which are more thermally broadened than the warm H₂ lines we study here, were unresolved in higher-resolution ($R \sim 4000$) Keck Cosmic Web

²<https://jwst.etc.stsci.edu>

³https://github.com/STScI-MIRI/MRS-ExampleNB/blob/main/Flight_Notebook1/MRS_FlightNB1.ipynb

Imager data [24]. Thus, we required the FWHM of the Gaussian emission-line model to be within 1% of the instrumental broadening, calculated at the wavelength (λ) of the S(1) line as $R = 4603 - 128(\lambda/\mu\text{m})$ [40]. The root-mean-square (RMS) error in the continuum level surrounding each line was adopted as a conservative estimate of the uncertainties on the observed surface brightness in our fitting with the `scipy.optimize.least_squares` routine in Python. We then calculated the S(1) line intensity in each spaxel as the area under the best-fit Gaussian model and propagated the uncertainties on the inferred parameters to determine the signal-to-noise ratio (S/N) of the measurement. After iterating over every spaxel in the channel 3 data cube across all 4 tiles in the mosaic, we found 6 contiguous spaxels with S(1) emission at $S/N > 3$. We then repeated this procedure to check each spaxel in the channel 3 and channel 2 data cubes for emission in the S(2) and S(3) lines, respectively, but found no significant detections. We also checked the channel 4 cube for S(0) emission, but found that the noise level was so high at wavelengths $\gtrsim 24 \mu\text{m}$ that any detection of, or useful limits on, the S(0) intensity would be impossible.

The spatial sampling of our reduced MIRI-MRS data cubes is finer than the spatial resolution of the instrument. We calculated the FWHM (θ , in arcseconds) of one resolution element at $17.03 \mu\text{m}$ as $\theta = 0.033(\lambda/\mu\text{m}) + 0.106$ [44]. The resulting $\theta = 0.67''$ corresponds to circular aperture covering the area of 8.8 spaxels (each $0.2''$ on a side in channel 3). Thus, the region where S(1) emission is detected is unresolved. To measure the average S(1) intensity, we took the average spectrum within the single spatial resolution element centered on the middle of the 6-spaxel region in which S(1) is significantly detected (i.e., within the white circle in the right panel of Figure 1), then fit a Gaussian plus continuum model to this higher-S/N average spectrum (see the left panel of Figure 2). Again, using the continuum RMS as the measurement uncertainty and standard error propagation techniques, we found a higher-significance S(1) detection at S/N of 5.3. We repeated that procedure to measure the S(2) and S(3) emission within the same region, but found that $S/N < 3$ for both lines in the averaged spectra. Thus, we placed $3\text{-}\sigma$ upper limits on those lines equal to 3 times the uncertainties we calculated on their best-fit intensities.

The S(3) transition falls in the shorter-wavelength channel 2, which has smaller spaxels ($0.17''$ on a side) and higher spatial resolution ($\theta = 0.42''$ at $9.66 \mu\text{m}$) than the channel 3 cube that covers both the S(1) and S(2) lines (Table 2). For consistency, we fixed the area over which we average the channel 2 spectrum to match that used for channel 3, though this is larger than one resolution element at the wavelength of S(3). We checked that averaging over a smaller area equal to one resolution element at $9.66 \mu\text{m}$ does not yield a significant detection of S(3) emission.

Warm H₂ Temperature and Mass Limits from the Rotational Lines

These measurements and upper limits on the H₂ rotational line strengths in Leo P constrain the temperature (T) and mass ($M_{\text{H}_2}^{\text{warm}}$) of the emitting warm H₂ [e.g., 45]. The intensity (I) of a given H₂ line is proportional to N_u , the column density of H₂ that is in the upper energy state of that transition. N_u is calculated from the observed line intensity as:

$$N_u = \frac{4\pi I}{A\Delta E} = \frac{4\pi I\lambda}{Ahc}, \quad (1)$$

where A is the Einstein coefficient (or emission probability; see Table 2) and the change in energy between the upper and lower levels of the transition, ΔE , is equal to hc/λ , where h is the Planck constant and c is the speed of light. The total column density (N) of the emitting warm H₂ across all energy states can be determined from a model of the form [e.g., 16]:

$$N_u = \frac{g_u N e^{-E_u/k_B T}}{Z(T)}, \quad (2)$$

where g_u is the statistical weight of the upper level (equal to $(2I + 1)(2J + 1)$, where J is the rotational quantum number and the total nuclear spin I is 0 for even- J transitions and 1 for odd J), E_u is the energy of the upper level, k_B is the Boltzmann constant, and $Z(T)$ is the partition function, which can be approximated accurately by [46]:

$$Z(T) = 0.024 T [1 - e^{-6000/T}]^{-1}. \quad (3)$$

The right panel of Figure 2 shows an excitation diagram constructed from our H₂ rotational line intensity measurements in Leo P. The utility of this $\ln(N_u/g_u)-E_u/k_B$ space becomes apparent when we rearrange Equation 2 and take the natural logarithm of both sides:

$$\ln(N_u/g_u) = -(1/T)(E_u/k_B) + \ln(N/Z(T)), \quad (4)$$

so T is equal to -1 divided by the slope of a linear model in the excitation diagram, and then N can be calculated from the intercept given that value of T . Because we only detected the S(1) line and placed upper limits on S(2) and S(3), we did not attempt to fit a linear model to the data in Figure 2. Instead, we constructed models varying T in steps of 10 K across the $T = 80$ –1000 K range over which H₂ is expected to produce detectable rotational emission [17, 45]. Then for each T , we calculated the range of N allowed within the uncertainties on the S(1) intensity measurement and the upper limit on the S(3) intensity, which is more constraining than the S(2) limit.

We found that models with $T > 420$ K are ruled out by the data, as such models that are consistent with the S(3) upper limit would predict a lower S(1) intensity than observed. This highest- T model also requires the lowest N to be consistent with our measurements (see Table 1), thus placing a lower limit on the warm H₂ present. Since this minimum N was measured from the averaged, spatially unresolved emission over one resolution element, we calculated the corresponding minimum $M_{\text{H}_2}^{\text{warm}}$ within the $0.67''$ FWHM (with a radius r equal to 2.63 pc at the distance of Leo P) as:

$$M_{\text{H}_2}^{\text{warm}} = N\pi r^2 m_{\text{H}_2}, \quad (5)$$

where m_{H_2} is the mass of an H₂ molecule, yielding a lower limit of $M_{\text{H}_2}^{\text{warm}} \geq 0.2 M_\odot$. But again, lower T and correspondingly higher N are allowed by the data, so the true warm H₂ content of Leo P could be much larger. Without a limit on the S(0) line intensity, we cannot determine the lowest allowed T of the emitting H₂, so adopt 80 K as a reasonable threshold below which the S(1) intensity is expected to drop off precipitously and become undetectable [17, 45]. If the true T of the emitting H₂ in Leo P were 80 K, then the maximum N consistent with our observations would correspond to $M_{\text{H}_2}^{\text{warm}} = 1.8 \times 10^3 M_\odot$. These H₂ mass estimates are only for the emitting, warm gas; yet, previous observations of star-forming galaxies at higher metallicity have demonstrated that ~ 10 –15% of the total H₂ mass is typically in the warm phase [16, 17]. Assuming that a similar temperature distribution holds at 3% Solar metallicity, then we can scale our $M_{\text{H}_2}^{\text{warm}}$ calculations to the implied minimum total (warm+cold) H₂ mass (M_{H_2}) using a total-to-warm H₂ ratio of 6.5. This results in M_{H_2} of $\geq 1.4 M_\odot$ for the lower-limit N corresponding to $T = 420$ K, or $1.1 \times 10^4 M_\odot$ if $T = 80$ K.

Finally, we note that though warm H₂ emission is often modeled as arising from two components at two different temperatures [e.g., the PDR Toolbox; 47–50], we have too few line detections to constrain all of the parameters in that more complex model, so we simply assume that all of the warm H₂ is at a single T . We also assume a fixed equilibrium ortho-to-para ratio of 3, as we do not have enough rotational line detections to include this as a free parameter in our model. While it is possible that the true value may be lower if the emitting H₂ is out of equilibrium or at a low temperature $\lesssim 200$ K [45], this assumption does not impact our conclusions. If the true ortho-to-para ratio is < 3 , then our measured N_u/g_u for the odd- J (ortho) transitions S(1) and S(3) would be underestimated by the same vertical offset in Figure 2 [e.g., 51]. Because our temperature constraint comes from the range of slopes allowed by the S(1) and S(3) data, it is unchanged by the implied change in normalization of the model. Our N_{tot} lower limits would change in the sense that the corrected values would be larger than what we report here, so the minimum warm and total M_{H_2} that we find in Leo P are conservatively small. Moreover, this is at most a factor of three effect because even at 80 K, the ortho-to-para ratio is ~ 1.1 [45].

Expected Warm H₂ Temperature from the O Star’s Ultraviolet Radiation

Observations of star-forming galaxies indicate that most of their H₂ rotational line emission is excited by massive stars illuminating molecular gas [e.g., 16]. Because Leo P contains only one O star at the center of its H II region, the ultraviolet radiation field illuminating the PDR where S(1) emission is detected is unusually well-constrained. We therefore used the observed properties of the O star to investigate what range of temperatures we should expect for the H₂ at the location of our detection.

We performed some exploratory PDR modeling using the simple hydrogen-carbon-oxygen chemical model described in Appendix A of [52], which is a modified version of a model originally introduced by [53]. In these initial calculations, we adopted a slab geometry and constant density (n) for the gas, and computed the temperature and chemical composition as a function of depth into the slab. To fix the strength of the illuminating radiation field, we adopted a separation of 4.4 pc between the O star and the slab, as suggested by the observed angular separation of $0.57''$. The true separation could be larger if the H₂-emitting gas lies in the foreground or background compared to the O star, but is unlikely to be significantly smaller. Using a model of the ultraviolet spectrum that was fit to the O star’s far-ultraviolet through near-infrared spectral energy distribution observed with the Hubble Space Telescope [23], we computed an incident photon flux of $F \simeq 1.8 \times 10^9 \text{ cm}^{-2} \text{ s}^{-1}$ in the 11.2–13.6 eV energy band at the position of the slab, corresponding to a radiation field strength of approximately $\chi \simeq 150$ in Habing units [54]. For the purposes of our modeling, we conservatively adopted a slightly larger field strength of $\chi = 200$ to account for the uncertainty in the exact location of the front of the slab.

We fixed the metallicity of the gas to 3% of the Solar value and assumed for simplicity that the elemental abundance ratio of C/O is the same as that in the local warm neutral medium [55]. We investigated the effect of adopting a smaller C/O ratio, and found that a factor of 2 decrease leads to a 25–30% higher temperature at the lowest densities, but negligible differences above $n \sim 1000 \text{ cm}^{-3}$. We also assumed a dust-to-gas ratio of 3% of the local value and adopted a treatment of photoelectric heating that assumes the presence of polycyclic aromatic hydrocarbons (PAHs) [56, 57]. In reality, it is plausible that the actual dust-to-gas ratio in Leo P is smaller than the value one gets by scaling linearly with metallicity [58] and it is also likely that photoheating from PAHs is negligible due to the sharp decrease in PAH abundance with metallicity [59–61]; both effects would reduce the photoelectric heating rate and hence reduce the gas temperature.

In Figure 3, we show the average temperature (T) of the slab as a function of n . These calculations assume a slab of thickness $L = 1 \text{ pc}$, but the results are insensitive to variations of a factor of 2 in this value. The average T shown here is weighted by H₂ S(1) emission, estimated assuming LTE level populations for the low-lying rotational levels of H₂. Weighting instead by H₂ mass yields similar results at $n < 10^4 \text{ cm}^{-3}$, but lower temperatures at higher densities where the mass-weighted average is primarily sensitive to the temperature of the cold H₂. We show results for two sets of calculations: one in which we fixed the cosmic ray ionisation rate of atomic hydrogen to a low value, $\zeta_{\text{H}} = 10^{-19} \text{ s}^{-1}$ (blue line) and a second in which we adopted a much larger value of $\zeta_{\text{H}} = 10^{-17} \text{ s}^{-1}$ (red line). Our choice of the low value here is designed to be representative of conditions in which we expect photoelectric heating to dominate, but our results are insensitive to the precise value chosen provided that $\zeta_{\text{H}} < 10^{-18} \text{ s}^{-1}$. Our choice of the high value is motivated by recent numerical simulations of star formation in a metal-poor system with a star formation rate two orders of magnitude higher than Leo P [62]. We see that heating by the photoelectric effect plus a low level of cosmic rays yields an average temperature that is less than 100 K at all densities considered here, suggesting that our S(1) detection is consistent with being produced in gas at the low end of the temperature range expected to excite H₂ rotational lines, given the properties of the O star. Significantly increasing the cosmic ray ionisation rate does produce gas with $T > 100 \text{ K}$ at densities below a few 1000 cm^{-3} , but even here the temperature is towards the bottom end of the range allowed by the S(1) detection and S(3) non-detection. We consider such a high value of ζ_{H} to be unlikely, given the low star formation rate of Leo P [63], but in the absence of a direct observational constraint, we cannot exclude this value. We also note that heating by an incident X-ray flux or by turbulent dissipation in shocks (if modeled as a uniform heating term) has a very similar effect.

Though we lack observational constraints on ζ_{H} or the turbulent dissipation rate, it is unlikely that cosmic rays, X-rays, or shocks contribute significantly to the PDR heating given the apparently simple environment in Leo P. Moreover, our modeling shows that even an implausibly high CR ionisation rate cannot produce temperatures at the high end of the range allowed by our observations of the H₂ rotational lines. Because the O star is expected to dominate the PDR heating, our modeling suggests that the temperature of the warm H₂ in Leo P is likely to be towards the lower end of the allowed range.

ALMA Observations and Upper Limits on L_{CO} and M_{H_2}

The ALMA observations of Leo P were taken on December 7th, 2014 (Project 2013.1.00397.S; PI: S. Warren) targeting the 115 GHz ¹²CO ($J=1-0$) line in band 3 with the 12m array and an integration time of 10705 s or 2.974 hours. The calibrators were J1058+0133 for the bandpass calibrator, Titan

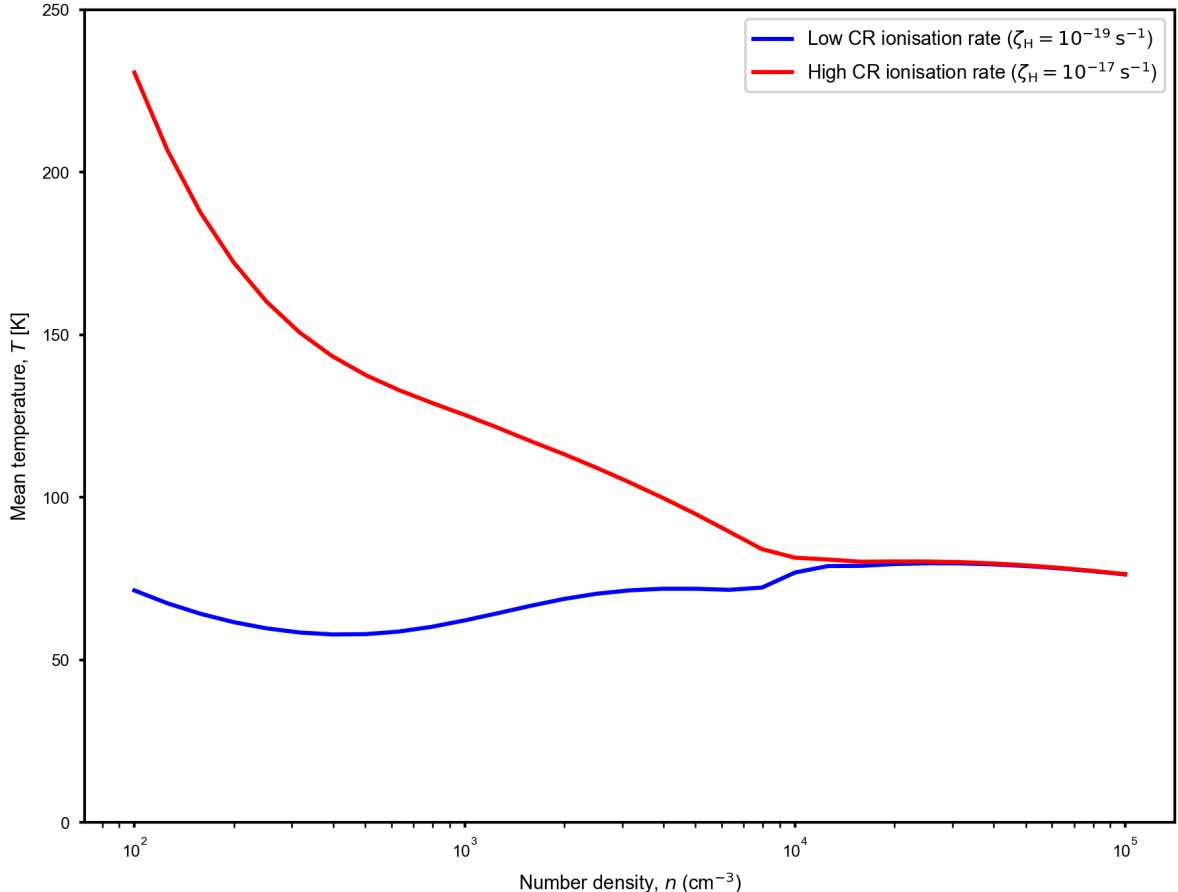


Fig. 3 H_2 S(1) emission-weighted mean temperature as a function of density for our simple one-dimensional PDR models of the warm H_2 in Leo P (see text for details). These calculations assume a slab symmetry for the emitting gas, with a thickness $L = 1$ pc and a uniform density as indicated in the figure. The slab is illuminated by the radiation field produced by the O star in Leo P, which has a strength of $\chi = 200$ in Habing units [54]. Results are shown for two different values for the cosmic ray (CR) ionisation rate: $\zeta_{\text{H}} = 10^{-19} \text{ s}^{-1}$ (blue line) and $\zeta_{\text{H}} = 10^{-17} \text{ s}^{-1}$ (red line).

for the flux calibrator, and J1012+2312 for the phase calibrator. The observations consisted of a single pointing that covered the peak of the H I distribution, where the field of view of the FWHM of the primary beam is shown as the red circle in Figure 1. We reimaged the raw calibrated data with version 4.2.2 of CASA (Common Astronomy Software Applications [64]) using the `clean` task and setting the image weight to natural weighting to optimize sensitivity. The restoring beam of the resulting data cube is $3.02''$ by $2.10''$ and the velocity resolution is 0.25 km s^{-1} . We find no robust $\text{CO}(1-0)$ detections in the data, and note that these ALMA observations are limited by the relatively large beam size of $3.02''$ by $2.10''$, which may dilute the emission from the very small ($< 1''$) CO clouds expected from the size of the H_2 region (see Figure 1). Still, we can use measurements of the noise to estimate a robust upper limit on the molecular gas mass in Leo P for comparison to the JWST MIRI-MRS detection of H_2 S(1) emission.

We took two approaches to estimate the upper limit on the CO luminosity (L_{CO}). The first approach follows a similar procedure to [7] and [65], enabling a direct comparison to the previous L_{CO} limit reported for Leo P. We smoothed the data cube to a velocity resolution of 2.5 km s^{-1} to match the average CO linewidth of molecular clouds observed in the low-metallicity galaxies WLM and Sextans B [8, 21], as well as the velocity resolution of H I observations of Leo P [30]. We calculated the upper limit on the CO intensity (S_{CO}) by measuring the RMS across the velocity channels that contain H I emission ($250 - 270 \text{ km s}^{-1}$), multiplied by the velocity channel width ($\Delta v = 2.5 \text{ km s}^{-1}$), then multiplied by a factor of 4 to achieve a $4\text{-}\sigma$ upper limit. The CO luminosity is given by:

$$L_{\text{CO}} = 2453D^2 S_{\text{CO}} = 9812D^2 \Delta v \text{ RMS} [\text{K km s}^{-1} \text{ pc}^2] \quad (6)$$

where the distance $D = 1.62 \text{ Mpc}$ (Table 1). The ALMA observations result in an upper limit of $L_{\text{CO}} \leq 83.4 \text{ K km s}^{-1} \text{ pc}^2$, which is almost two orders of magnitude deeper than the previous upper limit of $L_{\text{CO}} \leq 2900 \text{ K km s}^{-1} \text{ pc}^2$ presented in [7] using Combined Array for Millimeter-wave Astronomy (CARMA) observations of Leo P.

The second approach to calculate the L_{CO} upper limit uses a stacking procedure outlined in [66, 67] that assumes the velocity of any undetected CO clouds will be similar to the peak velocity of the H I emission, as is seen in other dwarf galaxies [e.g., 21, 67]. We first extracted a 100×100 pixel ($70'' \times 70''$) square region centered on the H II region and the H₂ S(1) detection. We regridded and interpolated the high-resolution $8''$ H I data cube presented in [30] to match the spectral resolution and pixel scale of the ALMA CO data cube. With the CO and H I data on the same frame, we fit the H I spectrum in a 10×10 pixel sub-region with a Gaussian model to identify the peak velocity. Each CO spectrum in a given sub-region was then shifted to this peak H I velocity and the process was repeated over the full 100-pixel-square region. We averaged the sub-region spectra to produce a final stacked spectrum, which decreased the noise by about a factor of 2. Using Equation 6, we calculated the $4\text{-}\sigma$ L_{CO} limit by measuring the RMS within the H I emission velocity bounds ($250\text{--}270 \text{ km s}^{-1}$) and the velocity resolution of the CO data ($\Delta v = 0.25 \text{ km s}^{-1}$) used in stacking. The final upper limit from stacking is $L_{\text{CO}} \leq 43.6 \text{ K km s}^{-1} \text{ pc}^2$, a factor of 2 lower than the upper limit calculated above. We adopt this upper limit from stacking in our calculations below as it is more sensitive than the traditional upper limit, which we report to facilitate comparison to the results in [7].

The observed L_{CO} is commonly used to determine the molecular hydrogen mass (M_{H_2}), but requires an assumption of a CO-to-H₂ conversion factor, α_{CO} :

$$M_{\text{H}_2} = \alpha_{\text{CO}} L_{\text{CO}}. \quad (7)$$

While $\alpha_{\text{CO}} = 4.3 M_{\odot} (\text{K km s}^{-1} \text{ pc}^2)^{-1}$ at Solar metallicity, the CO-to-H₂ conversion factor is known to vary substantially with metallicity [e.g., 15]. Galaxies with metallicities below Solar tend to have large reservoirs of “CO-dark” molecular gas, defined as areas of the interstellar medium where H₂ is present but the CO molecule is dissociated [e.g., 4, 14, 68–70]. It is therefore difficult to place a stringent constraint on the total molecular gas mass in an extremely low-metallicity galaxy like Leo P, particularly because it remains unclear how α_{CO} varies as a function of metallicity. To place a conservatively large upper limit on M_{H_2} , we use a theoretical CO-to-H₂ conversion factor from [4], whose 3% Solar metallicity models predict $\alpha_{\text{CO}} = 285 M_{\odot} (\text{K km s}^{-1} \text{ pc}^2)^{-1}$. This results in an upper limit of $M_{\text{H}_2} \leq 1.2 \times 10^4 M_{\odot}$ in Leo P, using the most sensitive L_{CO} limit from stacking. For comparison, adopting instead the $\alpha_{\text{CO}} = 70$ measured at 20% Solar metallicity in the Small Magellanic Cloud [31] would imply $M_{\text{H}_2} \leq 3.1 \times 10^3 M_{\odot}$, but α_{CO} is expected to be higher than this at the much lower 3% Solar metallicity of Leo P. Combining Leo P’s H I mass (Table 1) with the maximum M_{H_2} of $1.2 \times 10^4 M_{\odot}$ yields an upper limit on the molecular-to-atomic gas ratio of ≤ 0.015 , lower than the range observed in other nearby, star-forming dwarf galaxies [71].

Acknowledgements. Based on observations with the NASA/ESA James Webb Space Telescope obtained from MAST at the Space Telescope Science Institute, which is operated by the Association of Universities for Research in Astronomy, Incorporated, under NASA contract NAS5-26555. This paper makes use of ALMA data. ALMA is a partnership of ESO (representing its member states), NSF (USA) and NINS (Japan), together with NRC (Canada), MOST and ASIAA (Taiwan), and KASI (Republic of Korea), in cooperation with the Republic of Chile. The Joint ALMA Observatory is operated by ESO, AUI/NRAO and NAOJ. The National Radio Astronomy Observatory is a facility of the National Science Foundation operated under cooperative agreement by Associated Universities, Inc. This research used NASA Astrophysics Data System Bibliographic Services, adstex, and the arXiv preprint server. The following software was used in this analysis: Astropy [72–74], iPython [75], Matplotlib [76], NumPy [77, 78], SAOImageDS9 [79], SciPy [80], CASA [64], SpectralCube [81].

Funding. Support for this work was provided by NASA through grant JWST-GO-3449 from the Space Telescope Science Institute under NASA contract NAS5-26555. O. G. T. acknowledges support from a Carnegie-Princeton Fellowship through Princeton University and the Carnegie Observatories. This research was supported in part by grant NSF PHY-2309135 to the Kavli Institute for Theoretical Physics (KITP). S. C. O. G. acknowledges funding from the European Research Council via the ERC Synergy Grant “ECOGAL” (project ID 855130) and from the German Excellence Strategy via the Heidelberg

Cluster of Excellence “STRUCTURES” (EXC 2181 - 390900948). A. D. B. acknowledges support from the NSF under award AST-2108140.

Author contributions. O. G. T., K. M. S., and K. B. W. M. developed the idea for the JWST proposal. O. G. T. (PI of JWST-GO-3449) analyzed the H₂ emission lines in the MIRI-MRS observations of Leo P, made Figure 1 and Figure 2, and wrote the manuscript. K. M. S. led the design of the JWST observations and reduced the MIRI-MRS data. S. C. O. G. modeled the PDR to constrain the emitting H₂ temperature and made Figure 3. E. J. T. reduced the ALMA data and calculated the upper limit on L_{CO} in Leo P. All authors contributed to interpretation of the scientific results and to the manuscript.

Competing interests. The authors declare no competing interests.

Data availability. JWST MIRI-MRS data from program GO-3449 will be available to download from the Mikulski Archive for Space Telescopes (<https://mast.stsci.edu>) as of May 23, 2025. Data for ALMA Project 2013.1.00397.S are available to download from the ALMA Archive (<https://almascience.nrao.edu/alma-data>). Results from the PDR modeling are available from the authors on request. All other data in this paper have been previously published.

Code availability. Code to analyze the data and produce figures in this paper will be made available upon reasonable request to the corresponding author (O. G. T.; grace.telford@princeton.edu).

References

- [1] Labbé, I., van Dokkum, P., Nelson, E., Bezanson, R., Suess, K.A., Leja, J., Brammer, G., Whitaker, K., Mathews, E., Stefanon, M., Wang, B.: A population of red candidate massive galaxies 600 Myr after the Big Bang. *Nature* **616**(7956), 266–269 (2023) <https://doi.org/10.1038/s41586-023-05786-2> [arXiv:2207.12446](https://arxiv.org/abs/2207.12446) [astro-ph.GA]
- [2] Boylan-Kolchin, M.: Stress testing Λ CDM with high-redshift galaxy candidates. *Nature Astronomy* **7**, 731–735 (2023) <https://doi.org/10.1038/s41550-023-01937-7> [arXiv:2208.01611](https://arxiv.org/abs/2208.01611) [astro-ph.CO]
- [3] Carniani, S., Hainline, K., D’Eugenio, F., Eisenstein, D.J., Jakobsen, P., Witstok, J., Johnson, B.D., Chevillard, J., Maiolino, R., Helton, J.M., Willott, C., Robertson, B., Alberts, S., Arribas, S., Baker, W.M., Bhatawdekar, R., Boyett, K., Bunker, A.J., Cameron, A.J., Cargile, P.A., Charlot, S., Curti, M., Curtis-Lake, E., Egami, E., Giardino, G., Isaak, K., Ji, Z., Jones, G.C., Kumari, N., Maseda, M.V., Parlanti, E., Pérez-González, P.G., Rawle, T., Rieke, G., Rieke, M., Del Pino, B.R., Saxena, A., Scholtz, J., Smit, R., Sun, F., Tacchella, S., Übler, H., Venturi, G., Williams, C.C., Willmer, C.N.A.: Spectroscopic confirmation of two luminous galaxies at a redshift of 14. *Nature* **633**(8029), 318–322 (2024) <https://doi.org/10.1038/s41586-024-07860-9> [arXiv:2405.18485](https://arxiv.org/abs/2405.18485) [astro-ph.GA]
- [4] Glover, S.C.O., Clark, P.C.: Star formation in metal-poor gas clouds. *Mon. Not. R. Astron. Soc.* **426**(1), 377–388 (2012) <https://doi.org/10.1111/j.1365-2966.2012.21737.x> [arXiv:1203.4251](https://arxiv.org/abs/1203.4251) [astro-ph.GA]
- [5] Krumholz, M.R.: Star Formation in Atomic Gas. *Astrophys. J.* **759**(1), 9 (2012) <https://doi.org/10.1088/0004-637X/759/1/9> [arXiv:1208.1504](https://arxiv.org/abs/1208.1504) [astro-ph.CO]
- [6] Schinnerer, E., Leroy, A.K.: Molecular Gas and the Star-Formation Process on Cloud Scales in Nearby Galaxies. *Annu. Rev. Astron. Astrophys.* **62**(1), 369–436 (2024) <https://doi.org/10.1146/annurev-astro-071221-052651> [arXiv:2403.19843](https://arxiv.org/abs/2403.19843) [astro-ph.GA]
- [7] Warren, S.R., Molter, E., Cannon, J.M., Bolatto, A.D., Adams, E.A.K., Bernstein-Cooper, E.Z., Giovanelli, R., Haynes, M.P., Herrera-Camus, R., Jameson, K., McQuinn, K.B.W., Rhode, K.L., Salzer, J.J., Skillman, E.D.: CARMA CO Observations of Three Extremely Metal-poor, Star-forming Galaxies. *Astrophys. J.* **814**(1), 30 (2015) <https://doi.org/10.1088/0004-637X/814/1/30> [arXiv:1510.03518](https://arxiv.org/abs/1510.03518) [astro-ph.GA]
- [8] Shi, Y., Wang, J., Zhang, Z.-Y., Zhang, Q., Gao, Y., Zhou, L., Gu, Q., Qiu, K., Xia, X.-Y., Hao, C.-N., Chen, Y.: Oversized Gas Clumps in an Extremely Metal-poor Molecular Cloud Revealed by

- ALMA's Parsec-scale Maps. *Astrophys. J.* **892**(2), 147 (2020) <https://doi.org/10.3847/1538-4357/ab7a12> [arXiv:2002.10209](https://arxiv.org/abs/2002.10209) [astro-ph.GA]
- [9] Skillman, E.D., Salzer, J.J., Berg, D.A., Pogge, R.W., Haurberg, N.C., Cannon, J.M., Aver, E., Olive, K.A., Giovanelli, R., Haynes, M.P., Adams, E.A.K., McQuinn, K.B.W., Rhode, K.L.: ALFALFA Discovery of the nearby Gas-rich Dwarf Galaxy Leo P. III. An Extremely Metal Deficient Galaxy. *Astron. J.* **146**(1), 3 (2013) <https://doi.org/10.1088/0004-6256/146/1/3> [arXiv:1305.0277](https://arxiv.org/abs/1305.0277) [astro-ph.CO]
- [10] McQuinn, K.B.W., Skillman, E.D., Dolphin, A., Cannon, J.M., Salzer, J.J., Rhode, K.L., Adams, E.A.K., Berg, D., Giovanelli, R., Girardi, L., Haynes, M.P.: Leo P: An Unquenched Very Low-mass Galaxy. *Astrophys. J.* **812**(2), 158 (2015) <https://doi.org/10.1088/0004-637X/812/2/158> [arXiv:1506.05495](https://arxiv.org/abs/1506.05495) [astro-ph.GA]
- [11] Bolatto, A.D., Leroy, A.K., Jameson, K., Ostriker, E., Gordon, K., Lawton, B., Stanimirović, S., Israel, F.P., Madden, S.C., Hony, S., Sandstrom, K.M., Bot, C., Rubio, M., Winkler, P.F., Roman-Duval, J., van Loon, J.T., Oliveira, J.M., Indebetouw, R.: The State of the Gas and the Relation between Gas and Star Formation at Low Metallicity: The Small Magellanic Cloud. *Astrophys. J.* **741**(1), 12 (2011) <https://doi.org/10.1088/0004-637X/741/1/12> [arXiv:1107.1717](https://arxiv.org/abs/1107.1717) [astro-ph.CO]
- [12] Leroy, A.K., Walter, F., Sandstrom, K., Schrubba, A., Munoz-Mateos, J.-C., Bigiel, F., Bolatto, A., Brinks, E., de Blok, W.J.G., Meidt, S., Rix, H.-W., Rosolowsky, E., Schinnerer, E., Schuster, K.-F., Usero, A.: Molecular Gas and Star Formation in nearby Disk Galaxies. *Astron. J.* **146**(2), 19 (2013) <https://doi.org/10.1088/0004-6256/146/2/19> [arXiv:1301.2328](https://arxiv.org/abs/1301.2328) [astro-ph.CO]
- [13] Maloney, P., Black, J.H.: I CO/N(H 2) Conversions and Molecular Gas Abundances in Spiral and Irregular Galaxies. *Astrophys. J.* **325**, 389 (1988) <https://doi.org/10.1086/166011>
- [14] Wolfire, M.G., Hollenbach, D., McKee, C.F.: The Dark Molecular Gas. *Astrophys. J.* **716**(2), 1191–1207 (2010) <https://doi.org/10.1088/0004-637X/716/2/1191> [arXiv:1004.5401](https://arxiv.org/abs/1004.5401) [astro-ph.GA]
- [15] Bolatto, A.D., Wolfire, M., Leroy, A.K.: The CO-to-H₂ Conversion Factor. *Annu. Rev. Astron. Astrophys.* **51**(1), 207–268 (2013) <https://doi.org/10.1146/annurev-astro-082812-140944> [arXiv:1301.3498](https://arxiv.org/abs/1301.3498) [astro-ph.GA]
- [16] Roussel, H., Helou, G., Hollenbach, D.J., Draine, B.T., Smith, J.D., Armus, L., Schinnerer, E., Walter, F., Engelbracht, C.W., Thornley, M.D., Kennicutt, R.C., Calzetti, D., Dale, D.A., Murphy, E.J., Bot, C.: Warm Molecular Hydrogen in the Spitzer SINGS Galaxy Sample. *Astrophys. J.* **669**(2), 959–981 (2007) <https://doi.org/10.1086/521667> [arXiv:0707.0395](https://arxiv.org/abs/0707.0395) [astro-ph]
- [17] Togi, A., Smith, J.D.T.: Lighting the Dark Molecular Gas: H₂ as a Direct Tracer. *Astrophys. J.* **830**(1), 18 (2016) <https://doi.org/10.3847/0004-637X/830/1/18> [arXiv:1607.08036](https://arxiv.org/abs/1607.08036) [astro-ph.GA]
- [18] Hunt, L.K., Thuan, T.X., Izotov, Y.I., Sauvage, M.: The Spitzer View of Low-Metallicity Star Formation. III. Fine-Structure Lines, Aromatic Features, and Molecules. *Astrophys. J.* **712**(1), 164–187 (2010) <https://doi.org/10.1088/0004-637X/712/1/164> [arXiv:1002.0991](https://arxiv.org/abs/1002.0991) [astro-ph.CO]
- [19] Naslim, N., Kemper, F., Madden, S.C., Hony, S., Chu, Y.-H., Galliano, F., Bot, C., Yang, Y., Seok, J., Oliveira, J.M., van Loon, J.T., Meixner, M., Li, A., Hughes, A., Gordon, K.D., Otsuka, M., Hirashita, H., Morata, O., Lebouteiller, V., Indebetouw, R., Srinivasan, S., Bernard, J.-P., Reach, W.T.: Molecular hydrogen emission in the interstellar medium of the Large Magellanic Cloud. *Mon. Not. R. Astron. Soc.* **446**(3), 2490–2504 (2015) <https://doi.org/10.1093/mnras/stu2276> [arXiv:1407.7658](https://arxiv.org/abs/1407.7658) [astro-ph.GA]
- [20] McQuinn, K.B.W., Berg, D.A., Skillman, E.D., Adams, E.A.K., Cannon, J.M., Dolphin, A.E., Salzer, J.J., Giovanelli, R., Haynes, M.P., Hirschauer, A.S., Janoweicki, S., Klapkowski, M., Rhode, K.L.: The Leoncino Dwarf Galaxy: Exploring the Low-metallicity End of the Luminosity-Metallicity and

- Mass-Metallicity Relations. *Astrophys. J.* **891**(2), 181 (2020) <https://doi.org/10.3847/1538-4357/ab7447> arXiv:2002.11723 [astro-ph.GA]
- [21] Rubio, M., Elmegreen, B.G., Hunter, D.A., Brinks, E., Cortés, J.R., Cigan, P.: Dense cloud cores revealed by CO in the low metallicity dwarf galaxy WLM. *Nature* **525**(7568), 218–221 (2015) <https://doi.org/10.1038/nature14901> arXiv:1603.04736 [astro-ph.GA]
- [22] Evans, C.J., Castro, N., Gonzalez, O.A., Garcia, M., Bastian, N., Cioni, M.-R.L., Clark, J.S., Davies, B., Ferguson, A.M.N., Kamann, S., Lennon, D.J., Patrick, L.R., Vink, J.S., Weisz, D.R.: First stellar spectroscopy in Leo P. *Astron. Astrophys.* **622**, 129 (2019) <https://doi.org/10.1051/0004-6361/201834145> arXiv:1901.01295 [astro-ph.SR]
- [23] Telford, O.G., Chisholm, J., McQuinn, K.B.W., Berg, D.A.: Far-ultraviolet Spectra of Main-sequence O Stars at Extremely Low Metallicity. *Astrophys. J.* **922**(2), 191 (2021) <https://doi.org/10.3847/1538-4357/ac1ce2> arXiv:2109.06885 [astro-ph.SR]
- [24] Telford, O.G., McQuinn, K.B.W., Chisholm, J., Berg, D.A.: The Ionizing Spectra of Extremely Metal-poor O Stars: Constraints from the Only H II Region in Leo P. *Astrophys. J.* **943**(1), 65 (2023) <https://doi.org/10.3847/1538-4357/aca896> arXiv:2210.17535 [astro-ph.SR]
- [25] Telford, O.G., Chisholm, J., Sander, A.A.C., Ramachandran, V., McQuinn, K.B.W., Berg, D.A.: Observations of Extremely Metal-Poor O Stars: Weak Winds and Constraints for Evolution Models. arXiv e-prints, 2407–20313 (2024) <https://doi.org/10.48550/arXiv.2407.20313> arXiv:2407.20313 [astro-ph.SR]
- [26] McQuinn, K.B.W., Newman, M.J.B., Skillman, E.D., Telford, O.G., Brooks, A., Adams, E.A.K., Berg, D.A., Boyer, M.L., Cannon, J.M., Dolphin, A.E., Pahl, A., Rhode, K.L., Salzer, J.J., Cohen, R.E., Goldman, S.R.: The Ancient Star Formation History of the Extremely Low-Mass Galaxy Leo P: An Emerging Trend of a Post-Reionization Pause in Star Formation. arXiv e-prints, 2409–19050 (2024) arXiv:2409.19050 [astro-ph.GA]
- [27] Aloisi, A., Clementini, G., Tosi, M., Annibali, F., Contreras, R., Fiorentino, G., Mack, J., Marconi, M., Musella, I., Saha, A., Sirianni, M., van der Marel, R.P.: I Zw 18 Revisited with HST ACS and Cepheids: New Distance and Age. *Astrophys. J. Lett.* **667**(2), 151–154 (2007) <https://doi.org/10.1086/522368> arXiv:0707.2371 [astro-ph]
- [28] Izotov, Y.I., Lipovetsky, V.A., Chaffee, F.H., Foltz, C.B., Guseva, N.G., Kniazev, A.Y.: SBS 0335-052, A Probable Nearby Young Dwarf Galaxy: Evidence Pro and Con. *Astrophys. J.* **476**(2), 698–711 (1997) <https://doi.org/10.1086/303664> arXiv:astro-ph/9607119 [astro-ph]
- [29] Giovanelli, R., Haynes, M.P., Adams, E.A.K., Cannon, J.M., Rhode, K.L., Salzer, J.J., Skillman, E.D., Bernstein-Cooper, E.Z., McQuinn, K.B.W.: ALFALFA Discovery of the Nearby Gas-rich Dwarf Galaxy Leo P. I. H I Observations. *Astron. J.* **146**(1), 15 (2013) <https://doi.org/10.1088/0004-6256/146/1/15> arXiv:1305.0272 [astro-ph.CO]
- [30] Bernstein-Cooper, E.Z., Cannon, J.M., Elson, E.C., Warren, S.R., Chengular, J., Skillman, E.D., Adams, E.A.K., Bolatto, A.D., Giovanelli, R., Haynes, M.P., McQuinn, K.B.W., Pardy, S.A., Rhode, K.L., Salzer, J.J.: ALFALFA Discovery of the Nearby Gas-rich Dwarf Galaxy Leo P. V. Neutral Gas Dynamics and Kinematics. *Astron. J.* **148**(2), 35 (2014) <https://doi.org/10.1088/0004-6256/148/2/35> arXiv:1404.5298 [astro-ph.GA]
- [31] Leroy, A.K., Bolatto, A., Gordon, K., Sandstrom, K., Gratier, P., Rosolowsky, E., Engelbracht, C.W., Mizuno, N., Corbelli, E., Fukui, Y., Kawamura, A.: The CO-to-H₂ Conversion Factor from Infrared Dust Emission across the Local Group. *Astrophys. J.* **737**(1), 12 (2011) <https://doi.org/10.1088/0004-637X/737/1/12> arXiv:1102.4618 [astro-ph.CO]
- [32] Topping, M.W., Stark, D.P., Endsley, R., Plat, A., Whitler, L., Chen, Z., Charlot, S.: Searching for

- Extremely Blue UV Continuum Slopes at $z = 7-11$ in JWST/NIRCam Imaging: Implications for Stellar Metallicity and Ionizing Photon Escape in Early Galaxies. *Astrophys. J.* **941**(2), 153 (2022) <https://doi.org/10.3847/1538-4357/aca522> arXiv:2208.01610 [astro-ph.GA]
- [33] Atek, H., Labbé, I., Furtak, L.J., Chemerynska, I., Fujimoto, S., Setton, D.J., Miller, T.B., Oesch, P., Bezanson, R., Price, S.H., Dayal, P., Zitrin, A., Kokorev, V., Weaver, J.R., Brammer, G., Dokkum, P.v., Williams, C.C., Cutler, S.E., Feldmann, R., Fudamoto, Y., Greene, J.E., Leja, J., Maseda, M.V., Muzzin, A., Pan, R., Papovich, C., Nelson, E.J., Nanayakkara, T., Stark, D.P., Stefanon, M., Suess, K.A., Wang, B., Whitaker, K.E.: Most of the photons that reionized the Universe came from dwarf galaxies. *Nature* **626**(8001), 975–978 (2024) <https://doi.org/10.1038/s41586-024-07043-6> arXiv:2308.08540 [astro-ph.GA]
- [34] Christensen, C.R., Governato, F., Quinn, T., Brooks, A.M., Shen, S., McCleary, J., Fisher, D.B., Wadsley, J.: The effect of models of the interstellar media on the central mass distribution of galaxies. *Mon. Not. R. Astron. Soc.* **440**(3), 2843–2859 (2014) <https://doi.org/10.1093/mnras/stu399> arXiv:1211.0326 [astro-ph.CO]
- [35] Polzin, A., Kravtsov, A.V., Semenov, V.A., Gnedin, N.Y.: Modeling Molecular Hydrogen in Low-metallicity Galaxies. *Astrophys. J.* **966**(2), 172 (2024) <https://doi.org/10.3847/1538-4357/ad32cb> arXiv:2310.10712 [astro-ph.GA]
- [36] Rhode, K.L., Salzer, J.J., Haurberg, N.C., Van Sistine, A., Young, M.D., Haynes, M.P., Giovanelli, R., Cannon, J.M., Skillman, E.D., McQuinn, K.B.W., Adams, E.A.K.: ALFALFA Discovery of the Nearby Gas-rich Dwarf Galaxy Leo P. II. Optical Imaging Observations. *Astron. J.* **145**(6), 149 (2013) <https://doi.org/10.1088/0004-6256/145/6/149> arXiv:1305.0270 [astro-ph.GA]
- [37] Rieke, G.H., Wright, G.S., Böker, T., Bouwman, J., Colina, L., Glasse, A., Gordon, K.D., Greene, T.P., Güdel, M., Henning, T., Justtanont, K., Lagage, P.-O., Meixner, M.E., Nørgaard-Nielsen, H.-U., Ray, T.P., Ressler, M.E., van Dishoeck, E.F., Waelkens, C.: The Mid-Infrared Instrument for the James Webb Space Telescope, I: Introduction. *Publ. Astron. Soc. Pac.* **127**(953), 584 (2015) <https://doi.org/10.1086/682252> arXiv:1508.02294 [astro-ph.IM]
- [38] Wright, G.S., Rieke, G.H., Glasse, A., Ressler, M., García Marín, M., Aguilar, J., Alberts, S., Álvarez-Márquez, J., Argyriou, I., Banks, K., Baudoz, P., Boccaletti, A., Bouchet, P., Bouwman, J., Brandl, B.R., Breda, D., Bright, S., Cale, S., Colina, L., Cossou, C., Coulais, A., Cracraft, M., De Meester, W., Dicken, D., Engesser, M., Etxaluze, M., Fox, O.D., Friedman, S., Fu, H., Gasman, D., Gáspár, A., Gastaud, R., Geers, V., Glauser, A.M., Gordon, K.D., Greene, T., Greve, T.R., Grundy, T., Güdel, M., Guillard, P., Haderlein, P., Hashimoto, R., Henning, T., Hines, D., Holler, B., Detre, Ö.H., Jahromi, A., James, B., Jones, O.C., Justtanont, K., Kavanagh, P., Kendrew, S., Klaassen, P., Krause, O., Labiano, A., Lagage, P.-O., Lambros, S., Larson, K., Law, D., Lee, D., Libralato, M., Lorenzo Alvarez, J., Meixner, M., Morrison, J., Mueller, M., Murray, K., Mycroft, M., Myers, R., Nayak, O., Naylor, B., Nickson, B., Noriega-Crespo, A., Östlin, G., O’Sullivan, B., Ottens, R., Patapis, P., Penanen, K., Pietraszkiewicz, M., Ray, T., Regan, M., Roteliuk, A., Royer, P., Samara-Ratna, P., Samuelson, B., Sargent, B.A., Scheithauer, S., Schneider, A., Schreiber, J., Shaughnessy, B., Sheehan, E., Shivaee, I., Sloan, G.C., Tamas, L., Teague, K., Temim, T., Tikkanen, T., Tustain, S., van Dishoeck, E.F., Vandenbussche, B., Weilert, M., Whitehouse, P., Wolff, S.: The Mid-infrared Instrument for JWST and Its In-flight Performance. *Publ. Astron. Soc. Pac.* **135**(1046), 048003 (2023) <https://doi.org/10.1088/1538-3873/acbe66>
- [39] Wells, M., Pel, J.-W., Glasse, A., Wright, G.S., Aitink-Kroes, G., Azzollini, R., Beard, S., Brandl, B.R., Gallie, A., Geers, V.C., Glauser, A.M., Hastings, P., Henning, T., Jager, R., Justtanont, K., Kruijzinga, B., Lahuis, F., Lee, D., Martinez-Delgado, I., Martínez-Galarza, J.R., Meijers, M., Morrison, J.E., Müller, F., Nakos, T., O’Sullivan, B., Oudenhuisen, A., Parr-Burman, P., Pauwels, E., Rohloff, R.-R., Schmalzl, E., Sykes, J., Thelen, M.P., van Dishoeck, E.F., Vandenbussche, B., Venema, L.B., Visser, H., Waters, L.B.F.M., Wright, D.: The Mid-Infrared Instrument for the James Webb Space Telescope, VI: The Medium Resolution Spectrometer. *Publ. Astron. Soc. Pac.* **127**(953),

646 (2015) <https://doi.org/10.1086/682281> arXiv:1508.03070 [astro-ph.IM]

- [40] Argyriou, I., Glasse, A., Law, D.R., Labiano, A., Álvarez-Márquez, J., Patapis, P., Kavanagh, P.J., Gasman, D., Mueller, M., Larson, K., Vandenbussche, B., Glauser, A.M., Royer, P., Dicken, D., Harkett, J., Sargent, B.A., Engesser, M., Jones, O.C., Kendrew, S., Noriega-Crespo, A., Brandl, B., Rieke, G.H., Wright, G.S., Lee, D., Wells, M.: JWST MIRI flight performance: The Medium-Resolution Spectrometer. *Astron. Astrophys.* **675**, 111 (2023) <https://doi.org/10.1051/0004-6361/202346489> arXiv:2303.13469 [astro-ph.IM]
- [41] Bushouse, H., Eisenhamer, J., Dencheva, N., Davies, J., Greenfield, P., Morrison, J., Hodge, P., Simon, B., Grumm, D., Droettboom, M., Slavich, E., Sosey, M., Pauly, T., Miller, T., Jedrzejewski, R., Hack, W., Davis, D., Crawford, S., Law, D., Gordon, K., Regan, M., Cara, M., MacDonald, K., Bradley, L., Shanahan, C., Jamieson, W., Teodoro, M., Williams, T., Pena-Guerrero, M.: JWST Calibration Pipeline. <https://doi.org/10.5281/zenodo.12692459>
- [42] Spilker, J.S., Phadke, K.A., Aravena, M., Archipley, M., Bayliss, M.B., Birkin, J.E., Béthermin, M., Burgoyne, J., Cathey, J., Chapman, S.C., Dahle, H., Gonzalez, A.H., Gururajan, G., Hayward, C.C., Hezaveh, Y.D., Hill, R., Hutchison, T.A., Kim, K.J., Kim, S., Law, D., Legin, R., Malkan, M.A., Marrone, D.P., Murphy, E.J., Narayanan, D., Navarre, A., Olivier, G.M., Rich, J.A., Rigby, J.R., Reuter, C., Rhoads, J.E., Sharon, K., Smith, J.D.T., Solimano, M., Sulzenauer, N., Vieira, J.D., Vizgan, D., Weiß, A., Whitaker, K.E.: Spatial variations in aromatic hydrocarbon emission in a dust-rich galaxy. *Nature* **618**(7966), 708–711 (2023) <https://doi.org/10.1038/s41586-023-05998-6> arXiv:2306.03152 [astro-ph.GA]
- [43] Roueff, E., Abgrall, H., Czachorowski, P., Pachucki, K., Puchalski, M., Komasa, J.: The full infrared spectrum of molecular hydrogen. *Astron. Astrophys.* **630**, 58 (2019) <https://doi.org/10.1051/0004-6361/201936249> arXiv:1909.11585 [physics.atom-ph]
- [44] Law, D.R., E. Morrison, J., Argyriou, I., Patapis, P., Álvarez-Márquez, J., Labiano, A., Vandenbussche, B.: A 3D Drizzle Algorithm for JWST and Practical Application to the MIRI Medium Resolution Spectrometer. *Astron. J.* **166**(2), 45 (2023) <https://doi.org/10.3847/1538-3881/acdddc> arXiv:2306.05520 [astro-ph.IM]
- [45] Burton, M.G., Hollenbach, D.J., Tielens, A.G.G.: Mid-Infrared Rotational Line Emission from Interstellar Molecular Hydrogen. *Astrophys. J.* **399**, 563 (1992) <https://doi.org/10.1086/171947>
- [46] Herbst, T.M., Beckwith, S.V.W., Glindemann, A., Tacconi-Garman, L.E., Kroker, H., Krabbe, A.: A Near-Infrared Spectral Imaging Study of T Tau. *Astron. J.* **111**, 2403 (1996) <https://doi.org/10.1086/117974>
- [47] Kaufman, M.J., Wolfire, M.G., Hollenbach, D.J.: [Si II], [Fe II], [C II], and H₂ Emission from Massive Star-forming Regions. *Astrophys. J.* **644**(1), 283–299 (2006) <https://doi.org/10.1086/503596>
- [48] Pound, M.W., Wolfire, M.G.: The Photo Dissociation Region Toolbox. In: Argyle, R.W., Bunclark, P.S., Lewis, J.R. (eds.) *Astronomical Data Analysis Software and Systems XVII*. Astronomical Society of the Pacific Conference Series, vol. 394, p. 654 (2008)
- [49] Pound, M.W., Wolfire, M.G.: PDRT: Photo Dissociation Region Toolbox (2011)
- [50] Pound, M.W., Wolfire, M.G.: The PhotoDissociation Region Toolbox: Software and Models for Astrophysical Analysis. *Astron. J.* **165**(1), 25 (2023) <https://doi.org/10.3847/1538-3881/ac9b1f> arXiv:2210.08062 [astro-ph.IM]
- [51] Sheffer, Y., Wolfire, M.G., Hollenbach, D.J., Kaufman, M.J., Cordier, M.: PDR Model Mapping of Physical Conditions via Spitzer/IRS Spectroscopy of H₂: Theoretical Success toward NGC 2023-South. *Astrophys. J.* **741**(1), 45 (2011) <https://doi.org/10.1088/0004-637X/741/1/45> arXiv:1110.4614 [astro-ph.GA]

- [52] Hunter, G.H., Clark, P.C., Glover, S.C.O., Klessen, R.S.: Towards the impact of GMC collisions on the star formation rate. *Mon. Not. R. Astron. Soc.* **519**(3), 4152–4170 (2023) <https://doi.org/10.1093/mnras/stac3751> [arXiv:2109.06195](https://arxiv.org/abs/2109.06195) [astro-ph.GA]
- [53] Gong, M., Ostriker, E.C., Wolfire, M.G.: A Simple and Accurate Network for Hydrogen and Carbon Chemistry in the Interstellar Medium. *Astrophys. J.* **843**(1), 38 (2017) <https://doi.org/10.3847/1538-4357/aa7561> [arXiv:1610.09023](https://arxiv.org/abs/1610.09023) [astro-ph.GA]
- [54] Habing, H.J.: The interstellar radiation density between 912 Å and 2400 Å. *Bulletin of the Astronomical Institutes of the Netherlands* **19**, 421 (1968)
- [55] Sembach, K.R., Howk, J.C., Ryans, R.S.I., Keenan, F.P.: Modeling the Warm Ionized Interstellar Medium and Its Impact on Elemental Abundance Studies. *Astrophys. J.* **528**(1), 310–324 (2000) <https://doi.org/10.1086/308173> [arXiv:astro-ph/9908051](https://arxiv.org/abs/astro-ph/9908051) [astro-ph]
- [56] Bakes, E.L.O., Tielens, A.G.G.M.: The Photoelectric Heating Mechanism for Very Small Graphitic Grains and Polycyclic Aromatic Hydrocarbons. *Astrophys. J.* **427**, 822 (1994) <https://doi.org/10.1086/174188>
- [57] Wolfire, M.G., McKee, C.F., Hollenbach, D., Tielens, A.G.G.M.: Neutral Atomic Phases of the Interstellar Medium in the Galaxy. *Astrophys. J.* **587**(1), 278–311 (2003) <https://doi.org/10.1086/368016> [arXiv:astro-ph/0207098](https://arxiv.org/abs/astro-ph/0207098) [astro-ph]
- [58] Rémy-Ruyer, A., Madden, S.C., Galliano, F., Galametz, M., Takeuchi, T.T., Asano, R.S., Zhukovska, S., Lebouteiller, V., Cormier, D., Jones, A., Bocchio, M., Baes, M., Bendo, G.J., Boquien, M., Boselli, A., DeLooze, I., Doublier-Pritchard, V., Hughes, T., Karczewski, O.L., Spinoglio, L.: Gas-to-dust mass ratios in local galaxies over a 2 dex metallicity range. *Astron. Astrophys.* **563**, 31 (2014) <https://doi.org/10.1051/0004-6361/20132280310.48550> [arXiv:1312.3442](https://arxiv.org/abs/1312.3442) [arXiv:1312.3442](https://arxiv.org/abs/1312.3442) [astro-ph.GA]
- [59] Draine, B.T., Dale, D.A., Bendo, G., Gordon, K.D., Smith, J.D.T., Armus, L., Engelbracht, C.W., Helou, G., Kennicutt, J. R. C., Li, A., Roussel, H., Walter, F., Calzetti, D., Moustakas, J., Murphy, E.J., Rieke, G.H., Bot, C., Hollenbach, D.J., Sheth, K., Teplitz, H.I.: Dust Masses, PAH Abundances, and Starlight Intensities in the SINGS Galaxy Sample. *Astrophys. J.* **663**(2), 866–894 (2007) <https://doi.org/10.1086/51830610.48550> [arXiv:astro-ph/0703213](https://arxiv.org/abs/astro-ph/0703213) [arXiv:astro-ph/0703213](https://arxiv.org/abs/astro-ph/0703213) [astro-ph]
- [60] Engelbracht, C.W., Rieke, G.H., Gordon, K.D., Smith, J.-D.T., Werner, M.W., Moustakas, J., Willmer, C.N.A., Vanzi, L.: Metallicity Effects on Dust Properties in Starbursting Galaxies. *Astrophys. J.* **678**(2), 804–827 (2008) <https://doi.org/10.1086/52951310.48550> [arXiv:0801.1700](https://arxiv.org/abs/0801.1700) [astro-ph]
- [61] Whitcomb, C.M., Smith, J.-D.T., Sandstrom, K., Starkey, C.A., Donnelly, G.P., Draine, B.T., Skillman, E.D., Dale, D.A., Armus, L., Hensley, B.S., Lai, T.S.-Y., Kennicutt, R.C.: The Metallicity Dependence of PAH Emission in Galaxies I: Insights from Deep Radial Spitzer Spectroscopy. *arXiv e-prints*, 2405–09685 (2024) <https://doi.org/10.48550/arXiv.2405.09685> [arXiv:2405.09685](https://arxiv.org/abs/2405.09685) [astro-ph.GA]
- [62] Hu, C.-Y., Sternberg, A., van Dishoeck, E.F.: Coevolution of Dust and Chemistry in Galaxy Simulations with a Resolved Interstellar Medium. *Astrophys. J.* **952**(2), 140 (2023) <https://doi.org/10.3847/1538-4357/acdcfa> [arXiv:2301.05247](https://arxiv.org/abs/2301.05247) [astro-ph.GA]
- [63] Girichidis, P., Offner, S.S.R., Kritsuk, A.G., Klessen, R.S., Hennebelle, P., Kruijssen, J.M.D., Krause, M.G.H., Glover, S.C.O., Padovani, M.: Physical Processes in Star Formation. *Space Sci. Rev.* **216**(4), 68 (2020) <https://doi.org/10.1007/s11214-020-00693-8> [arXiv:2005.06472](https://arxiv.org/abs/2005.06472) [astro-ph.GA]
- [64] CASA Team, Bean, B., Bhatnagar, S., Castro, S., Donovan Meyer, J., Emonts, B., Garcia, E., Garwood, R., Golap, K., Gonzalez Villalba, J., Harris, P., Hayashi, Y., Hoskins, J., Hsieh, M., Jagannathan, P., Kawasaki, W., Keimpema, A., Kettenis, M., Lopez, J., Marvil, J., Masters, J.,

- McNichols, A., Mehringer, D., Miel, R., Moellenbrock, G., Montesino, F., Nakazato, T., Ott, J., Petry, D., Pokorny, M., Raba, R., Rau, U., Schiebel, D., Schweighart, N., Sekhar, S., Shimada, K., Small, D., Steeb, J.-W., Sugimoto, K., Suoranta, V., Tsutsumi, T., van Bemmell, I.M., Verkouter, M., Wells, A., Xiong, W., Szomoru, A., Griffith, M., Glendenning, B., Kern, J.: CASA, the Common Astronomy Software Applications for Radio Astronomy. *Publ. Astron. Soc. Pac.* **134**(1041), 114501 (2022) <https://doi.org/10.1088/1538-3873/ac9642> arXiv:2210.02276 [astro-ph.IM]
- [65] Leroy, A., Cannon, J., Walter, F., Bolatto, A., Weiss, A.: The Low CO Content of the Extremely Metal-poor Galaxy I Zw 18. *Astrophys. J.* **663**(2), 990–994 (2007) <https://doi.org/10.1086/518501> arXiv:0704.0862 [astro-ph]
- [66] Schruba, A., Leroy, A.K., Walter, F., Bigiel, F., Brinks, E., de Blok, W.J.G., Dumas, G., Kramer, C., Rosolowsky, E., Sandstrom, K., Schuster, K., Usero, A., Weiss, A., Wiesemeyer, H.: A Molecular Star Formation Law in the Atomic-gas-dominated Regime in Nearby Galaxies. *Astron. J.* **142**(2), 37 (2011) <https://doi.org/10.1088/0004-6256/142/2/37> arXiv:1105.4605 [astro-ph.CO]
- [67] Schruba, A., Leroy, A.K., Walter, F., Bigiel, F., Brinks, E., de Blok, W.J.G., Kramer, C., Rosolowsky, E., Sandstrom, K., Schuster, K., Usero, A., Weiss, A., Wiesemeyer, H.: Low CO Luminosities in Dwarf Galaxies. *Astron. J.* **143**(6), 138 (2012) <https://doi.org/10.1088/0004-6256/143/6/138> arXiv:1203.4231 [astro-ph.CO]
- [68] Grenier, I.A., Casandjian, J.-M., Terrier, R.: Unveiling Extensive Clouds of Dark Gas in the Solar Neighborhood. *Science* **307**(5713), 1292–1295 (2005) <https://doi.org/10.1126/science.1106924>
- [69] Jameson, K.E., Bolatto, A.D., Wolfire, M., Warren, S.R., Herrera-Camus, R., Croxall, K., Pellegrini, E., Smith, J.-D., Rubio, M., Indebetouw, R., Israel, F.P., Meixner, M., Roman-Duval, J., van Loon, J.T., Muller, E., Verdugo, C., Zinnecker, H., Okada, Y.: First Results from the Herschel and ALMA Spectroscopic Surveys of the SMC: The Relationship between [C II]-bright Gas and CO-bright Gas at Low Metallicity. *Astrophys. J.* **853**(2), 111 (2018) <https://doi.org/10.3847/1538-4357/aaa4bb> arXiv:1801.03518 [astro-ph.GA]
- [70] Madden, S.C., Cormier, D., Hony, S., Lebouteiller, V., Abel, N., Galametz, M., De Looze, I., Chevance, M., Polles, F.L., Lee, M.-Y., Galliano, F., Lambert-Huyghe, A., Hu, D., Ramambason, L.: Tracing the total molecular gas in galaxies: [CII] and the CO-dark gas. *Astron. Astrophys.* **643**, 141 (2020) <https://doi.org/10.1051/0004-6361/202038860> arXiv:2009.00649 [astro-ph.GA]
- [71] Leroy, A.K., Walter, F., Bigiel, F., Usero, A., Weiss, A., Brinks, E., de Blok, W.J.G., Kennicutt, R.C., Schuster, K.-F., Kramer, C., Wiesemeyer, H.W., Roussel, H.: Heracles: The HERA CO Line Extragalactic Survey. *Astron. J.* **137**(6), 4670–4696 (2009) <https://doi.org/10.1088/0004-6256/137/6/4670> arXiv:0905.4742 [astro-ph.CO]
- [72] Astropy Collaboration, Robitaille, T.P., Tollerud, E.J., Greenfield, P., Droettboom, M., Bray, E., Aldcroft, T., Davis, M., Ginsburg, A., Price-Whelan, A.M., Kerzendorf, W.E., Conley, A., Crighton, N., Barbary, K., Muna, D., Ferguson, H., Grollier, F., Parikh, M.M., Nair, P.H., Unther, H.M., Deil, C., Woillez, J., Conseil, S., Kramer, R., Turner, J.E.H., Singer, L., Fox, R., Weaver, B.A., Zabalza, V., Edwards, Z.I., Azalee Bostroem, K., Burke, D.J., Casey, A.R., Crawford, S.M., Dencheva, N., Ely, J., Jenness, T., Labrie, K., Lim, P.L., Pierfederici, F., Pontzen, A., Ptak, A., Retsdal, B., Servillat, M., Streicher, O.: Astropy: A community Python package for astronomy. *Astron. Astrophys.* **558**, 33 (2013) <https://doi.org/10.1051/0004-6361/201322068> arXiv:1307.6212 [astro-ph.IM]
- [73] Astropy Collaboration, Price-Whelan, A.M., Sipőcz, B.M., Günther, H.M., Lim, P.L., Crawford, S.M., Conseil, S., Shupe, D.L., Craig, M.W., Dencheva, N., Ginsburg, A., VanderPlas, J.T., Bradley, L.D., Pérez-Suárez, D., de Val-Borro, M., Aldcroft, T.L., Cruz, K.L., Robitaille, T.P., Tollerud, E.J., Ardelean, C., Babej, T., Bach, Y.P., Bachetti, M., Bakanov, A.V., Bamford, S.P., Barentsen, G., Barmby, P., Baumbach, A., Berry, K.L., Biscani, F., Boquien, M., Bostroem, K.A., Bouma, L.G., Brammer, G.B., Bray, E.M., Breytenbach, H., Buddelmeijer, H., Burke, D.J., Calderone, G., Cano Rodríguez, J.L., Cara, M., Cardoso, J.V.M., Cheedella, S., Copin, Y., Corrales, L., Crichton, D.,

- D'Avella, D., Deil, C., Depagne, É., Dietrich, J.P., Donath, A., Droettboom, M., Earl, N., Erben, T., Fabbro, S., Ferreira, L.A., Finethy, T., Fox, R.T., Garrison, L.H., Gibbons, S.L.J., Goldstein, D.A., Gommers, R., Greco, J.P., Greenfield, P., Groener, A.M., Grollier, F., Hagen, A., Hirst, P., Homeier, D., Horton, A.J., Hosseinzadeh, G., Hu, L., Hunkeler, J.S., Ivezić, Ž., Jain, A., Jenness, T., Kanarek, G., Kendrew, S., Kern, N.S., Kerzendorf, W.E., Khvalko, A., King, J., Kirkby, D., Kulkarni, A.M., Kumar, A., Lee, A., Lenz, D., Littlefair, S.P., Ma, Z., Macleod, D.M., Mastropietro, M., McCully, C., Montagnac, S., Morris, B.M., Mueller, M., Mumford, S.J., Muna, D., Murphy, N.A., Nelson, S., Nguyen, G.H., Ninan, J.P., Nöthe, M., Ogaz, S., Oh, S., Parejko, J.K., Parley, N., Pascual, S., Patil, R., Patil, A.A., Plunkett, A.L., Prochaska, J.X., Rastogi, T., Reddy Janga, V., Sabater, J., Sakurikar, P., Seifert, M., Sherbert, L.E., Sherwood-Taylor, H., Shih, A.Y., Sick, J., Silbiger, M.T., Singanamalla, S., Singer, L.P., Sladen, P.H., Sooley, K.A., Sornarajah, S., Streicher, O., Teuben, P., Thomas, S.W., Tremblay, G.R., Turner, J.E.H., Terrón, V., van Kerkwijk, M.H., de la Vega, A., Watkins, L.L., Weaver, B.A., Whitmore, J.B., Woillez, J., Zabalza, V., Astropy Contributors: The Astropy Project: Building an Open-science Project and Status of the v2.0 Core Package. *Astron. J.* **156**(3), 123 (2018) <https://doi.org/10.3847/1538-3881/aabc4f> arXiv:1801.02634 [astro-ph.IM]
- [74] Aver, E., Berg, D.A., Hirschauer, A.S., Olive, K.A., Pogge, R.W., Rogers, N.S.J., Salzer, J.J., Skillman, E.D.: A comprehensive chemical abundance analysis of the extremely metal poor Leoncino Dwarf galaxy (AGC 198691). *Mon. Not. R. Astron. Soc.* **510**(1), 373–382 (2022) <https://doi.org/10.1093/mnras/stab3226> arXiv:2109.00178 [astro-ph.GA]
- [75] Perez, F., Granger, B.E.: IPython: A System for Interactive Scientific Computing. *Computing in Science and Engineering* **9**(3), 21–29 (2007) <https://doi.org/10.1109/MCSE.2007.53>
- [76] Hunter, J.D.: Matplotlib: A 2D Graphics Environment. *Computing in Science and Engineering* **9**(3), 90–95 (2007) <https://doi.org/10.1109/MCSE.2007.55>
- [77] van der Walt, S., Colbert, S.C., Varoquaux, G.: The NumPy Array: A Structure for Efficient Numerical Computation. *Computing in Science and Engineering* **13**(2), 22–30 (2011) <https://doi.org/10.1109/MCSE.2011.37> arXiv:1102.1523 [cs.MS]
- [78] Harris, C.R., Millman, K.J., van der Walt, S.J., Gommers, R., Virtanen, P., Cournapeau, D., Wieser, E., Taylor, J., Berg, S., Smith, N.J., Kern, R., Picus, M., Hoyer, S., van Kerkwijk, M.H., Brett, M., Haldane, A., del Río, J.F., Wiebe, M., Peterson, P., Gérard-Marchant, P., Sheppard, K., Reddy, T., Weckesser, W., Abbasi, H., Gohlke, C., Oliphant, T.E.: Array programming with NumPy. *Nature* **585**(7825), 357–362 (2020) <https://doi.org/10.1038/s41586-020-2649-2> arXiv:2006.10256 [cs.MS]
- [79] Joye, W.A., Mandel, E.: New Features of SAOImage DS9. In: Payne, H.E., Jedrzejewski, R.I., Hook, R.N. (eds.) *Astronomical Data Analysis Software and Systems XII*. Astronomical Society of the Pacific Conference Series, vol. 295, p. 489 (2003)
- [80] Virtanen, P., Gommers, R., Oliphant, T.E., Haberland, M., Reddy, T., Cournapeau, D., Burovski, E., Peterson, P., Weckesser, W., Bright, J., van der Walt, S.J., Brett, M., Wilson, J., Millman, K.J., Mayorov, N., Nelson, A.R.J., Jones, E., Kern, R., Larson, E., Carey, C.J., Polat, I., Feng, Y., Moore, E.W., VanderPlas, J., Laxalde, D., Perktold, J., Cimrman, R., Henriksen, I., Quintero, E.A., Harris, C.R., Archibald, A.M., Ribeiro, A.H., Pedregosa, F., van Mulbregt, P., SciPy 1.0 Contributors: SciPy 1.0: fundamental algorithms for scientific computing in Python. *Nature Methods* **17**, 261–272 (2020) <https://doi.org/10.1038/s41592-019-0686-2> arXiv:1907.10121 [cs.MS]
- [81] Ginsburg, A., Koch, E., Robitaille, T., Beaumont, C., Adamginsburg, ZuHone, J., Sipocz, B., Patra, S., Jones, C., Lim, P.L., Rosolowsky, E., Stern, K., Earl, N., De Val-Borro, M., Jrobbed, Shuokong, Kepley, A., Sokolov, V., Badger, T.G., Maret, S., Garrido, J., Booker, J., Tollerud, E.: Radio-astro-tools/spectral-cube: V0.4.4. <https://doi.org/10.5281/zenodo.2573901>